THE ASTROPHYSICAL JOURNAL, 518:821–832, 1999 June 20

SIMILARITY CRITERIA FOR THE LABORATORY SIMULATION OF SUPERNOVA HYDRODYNAMICS

D. RYUTOV, R. P. DRAKE,[1] J. KANE, E. LIANG,[2] B. A. REMINGTON, AND W. M. WOOD-VASEY[3]
Lawrence Livermore National Laboratory, Livermore, CA 94551
Received 1998 June 11; accepted 1999 January 21

ABSTRACT

The conditions for validity and the limitations of experiments intended to simulate astrophysical hydrodynamics are discussed, with application to some ongoing experiments. For systems adequately described by the Euler equations, similarity criteria required for properly scaled experiments are identified. The conditions for the applicability of the Euler equations are formulated, based on the analysis of localization, heat conduction, viscosity, and radiation. Other considerations involved in such a scaling, including its limitations at small spatial scales, are discussed. The results are applied to experiments aimed at simulating three-dimensional hydrodynamics during supernova explosions and hydrodynamic instabilities in young supernova remnants. In addition, hydrodynamic situations with significant radiative effects are discussed.

Subject headings: hydrodynamics — instabilities — shock waves — supernova remnants — supernovae: general — supernovae: individual (SN 1987A)

1. INTRODUCTION

The explosion of a supernova (SN) involves a great variety of physical processes occurring on very disparate temporal and spatial scales. Our prime interest in this work is in a well-defined specific group of problems: hydrodynamic effects accompanying the SN explosion and subsequent expansion. Among the most interesting and important hydrodynamic phenomena are instabilities caused by the presence of continuous or impulsive acceleration of the fluid with radially varying density, namely, the Rayleigh-Taylor and Richtmyer-Meshkov instabilities. Another fundamentally important and interesting issue is the role of radiation in the dynamics of the evolving plasmas. To accomplish laboratory experiments that are a scaled simulation of SN hydrodynamic phenomena is a very challenging problem. At first, it might seem that laboratory simulations are impossible, in particular because of the enormous difference in the scales. However, first steps (Kane et al. 1997; Remington et al. 1997a, 1997b; Drake et al. 1998; Liang 1996) have been made in this direction with the use of the Nova laser facility. Here we establish, formally, the conditions for validity and the limitations of such laboratory simulation experiments.

In this paper we discuss the similarity criteria that define the parameter domain for scaled simulation experiments. While our analysis of the scaling from the laboratory to SNe and supernova remnants (SNRs) is quite general, we choose two specific examples relevant to SN 1987A for in-depth discussion. Indeed, the large amount of observational data obtained during the last decade from SN 1987A in the Large Magellanic Cloud, and the excitement concerning the impending collision of the blast wave with the ringlike circumstellar nebular object situated at a distance of $\sim 5 \times 10^{17}$ cm from the star, make this SN a natural reference point for numerical estimates. The general morphology of the SN 1987A event is described in several surveys, e.g., Arnett et al. (1989), Hillebrandt & Höflich (1989), Chevalier (1992), and McCray (1993). Important results regarding hydrodynamic aspects of the 1987 supernova can be found in Muller, Fryxell, & Arnett (1991), Chevalier (1992), and Chevalier, Blondin, & Emmering (1992).

In § 2 of the paper, we analyse the problem of scaling between two systems for the study of hydrodynamic effects. We discuss first the hydrodynamic problem, identifying scaling relations from the Euler equations that establish a connection we describe as Euler similarity. We then consider the conditions that must be met for such a hydrodynamic scaling to be valid. After that, we seek the limits of such similarity, in particular, to quantify the small spatial scale on which it breaks down.

In § 3 we apply these results to three phases of the SN 1987A explosion: expansion of the progenitor star under the action of the core explosion, interaction of the expanding SN ejecta with the circumstellar medium, and the collision of the expanding blast wave with the circumstellar ring. As a reference point for the first (explosion) phase, we consider the moment when the shock wave has propagated approximately halfway through the progenitor, which occurs a few thousand seconds after the explosion. As a reference point for the second phase, we take the time approximately 13 years after the explosion, just before the shock wave generated in the circumstellar medium reaches the circumstellar ring of SN 1987A. As a reference point for the third phase, we take the time of the collision of the blast wave with the circumstellar ring nebula. We close § 3 with a discussion of the requirements for producing hydrodynamic conditions where radiative effects are important.

During all three phases outlined above, the regions of interest are in the state of an ionized and highly conductive medium. Therefore, effects of a magnetic field may be important and should be taken into consideration. To be sure that the magnetic field does not have a "dynamic" influence on the hydrodynamics of the system under study, the magnetic field should be below some upper level determined by the plasma pressure or the kinetic energy of hydrodynamic motions. This condition is satisfied with a large margin at all three stages of the SN 1987A explosion discussed here. Accordingly, ordinary hydrodynamics, without magnetic stresses included, can be used.

[1] Atmospheric, Oceanic, and Space Sciences, University of Michigan, Ann Arbor, MI 48105.
[2] Rice University, Houston, TX 77251.
[3] Harvey Mudd College, Claremont, CA 91711.

At the same time, during the second and the third phases discussed here (SNR expansion and collision with ring) the magnetic field should exceed a certain level required to restore the "effective" collisionality in the otherwise essentially collisionless plasma. As we discuss later in the paper, the magnetic field in the SN ejecta and in the circumstellar plasma do exceed this limit. Therefore, the approach based on the use of ordinary hydrodynamics seems to be adequate in the analysis of the SN dynamics at all three stages discussed here.

Our paper is devised to provide a framework that will allow one, with a reasonable degree of confidence, to establish links between an experiment and an astrophysical system. Therefore, we do not present or discuss in any detail results of specific numerical simulations of either the laser experiment or the supernova event; rather, we use characteristic parameters based on SN 1987A as a reference point.

We use predominantly the cgs (Gaussian) system, of units. The temperature is measured in the energy units ($k_{\rm Boltzmann} = 1$). In "practical" numerical estimates we use mixed units, which are specified in each case. In the following, § 2 discusses the scaling between laboratory and astrophysical systems. Section 3 applies these results to the simulation of an SN, an SNR, and a ring collision, as well as to the simulation of radiative conditions.

2. THE SCALING PROBLEM

2.1. *Conditions for Hydrodynamic Similarity*

We first discuss the conditions under which two systems will behave identically, on the assumption (discussed later) that they behave as ideal (i.e., with zero viscosity and thermal conductivity) compressible hydrodynamic fluids whose evolution is described by the Euler equations. We later discuss the assumptions that heat transport and viscous momentum transport are unimportant.

With respect to thermodynamic properties of the matter, we limit ourselves to the case of a so-called polytropic gas (e.g., Landau & Lifshitz 1987), in which the energy density per unit volume, ε, is proportional to the pressure, p: $\varepsilon = \text{constant} \times p$. Note that this assumption goes beyond the assumption of a thermodynamically ideal gas. In particular, it breaks down for a gas with internal degrees of freedom that are excited at higher temperatures. It is, however, a good approximation for a fully ionized gas and for a gas dominated by radiative pressure. For an adiabatic process in a gas with $\varepsilon = \text{constant} \times p$, one has $p \propto \rho^\gamma$, with the adiabatic index $\gamma = 1 + (1/\text{constant})$.

The Euler equations for the polytropic gas read (e.g., Landau & Lifshitz 1987)

$$\rho\left(\frac{\partial \boldsymbol{v}}{\partial t} + \boldsymbol{v} \cdot \nabla \boldsymbol{v}\right) = -\nabla p\,,$$

$$\frac{\partial \rho}{\partial t} + \nabla \cdot (\rho \boldsymbol{v}) = 0\,,$$

$$\frac{\partial p}{\partial t} - \gamma \frac{p}{\rho}\frac{\partial \rho}{\partial t} + \boldsymbol{v} \cdot \nabla p - \gamma \frac{p}{\rho} \boldsymbol{v} \cdot \nabla \rho = 0\,, \tag{1}$$

in which ρ is the density, $\boldsymbol{v}$ is the fluid velocity, and γ is an adiabatic index. The first of these equations is the momentum balance equation, the second is the continuity equation, and the third is an entropy conservation equation for a polytropic gas.

Equations (1) remain invariant under the transformation (bearing the subscript 1):

$$\boldsymbol{r} = a\boldsymbol{r}_1\,; \quad \rho = b\rho_1\,; \quad p = cp_1\,;$$

$$t = a\sqrt{\frac{b}{c}}\,t_1\,; \quad \boldsymbol{v} = \sqrt{\frac{c}{b}}\,\boldsymbol{v}_1\,, \tag{2}$$

where a, b, and c are arbitrary positive numbers. There is thus a direct correspondence between any two systems satisfying equation (2). The matching conditions at the surface of the shock wave are also invariant under the transformation of equation (2). Therefore, the presence of hydrodynamic shocks of arbitrary strength is allowed. We will refer to the similarity described by equations (2) as the "Euler similarity," since it follows directly from the Euler equations. This similarity is more or less obvious from the general viewpoint (Zeldovich & Raizer 1966; Sedov 1997), although we have not found it discussed in the published literature. What is important for our purposes is that it covers all the aspects of the hydrodynamic instability of the SN: both Richtmeyer-Meshkov and Rayleigh-Taylor, both at their linear and nonlinear stages, with their possible interaction with the Kelvin-Helmholtz instability, and with full allowance for the compressibility of the medium.

Consider the Euler similarity in an initial-value problem for a closed hydrodynamic system. Take some initial state of the system, where the velocity, pressure, and density are

$$\boldsymbol{v}|_{t=0} = \tilde{v}\boldsymbol{F}(\boldsymbol{r}/h)\,, \quad p|_{t=0} = \tilde{p}G(\boldsymbol{r}/h)\,,$$

$$\rho|_{t=0} = \tilde{\rho}H(\boldsymbol{r}/h)\,, \tag{3}$$

with some dimensionless functions $\boldsymbol{F}$, G, and H. The multipliers $\tilde{v}$, $\tilde{p}$, $\tilde{\rho}$, as well as the quantity h, are scaling factors. Consider now another system, where the functions $\boldsymbol{F}$, G, and H remain the same (i.e., the initial state is geometrically similar to the state of the first system), but the scaling factors are different ($\tilde{v}_1$, $\tilde{p}_1$, $\tilde{\rho}_1$, and h_1). According to the last relationship of equation (2), the two systems will behave similarly if the equality

$$\tilde{v}\sqrt{\frac{\tilde{\rho}}{\tilde{p}}} = \tilde{v}_1\sqrt{\frac{\tilde{\rho}_1}{\tilde{p}_1}} \tag{4}$$

holds. This equality ensures the similar behavior of the two systems (provided the initial conditions are geometrically similar). In choosing where to normalize the functions $\boldsymbol{F}$, G, and H, it is useful to select locations that reflect the problem under study. Thus, if the instability of a specific interface is of interest, then taking $\tilde{v}$, $\tilde{\rho}$, and $\tilde{p}$ near that interface is appropriate. This is illustrated in the specific cases discussed in later sections. The quantity $\tilde{v}(\tilde{\rho}/\tilde{p})^{1/2}$ is similar to a Mach number, but need not correspond to any specific Mach number in a given problem. We suggest that it might be called the Euler number, that is, $\text{Eu} = \tilde{v}(\tilde{\rho}/\tilde{p})^{1/2}$.

If one compares the evolution of two systems, similar in the sense of equation (4), and having spatial scales h and h_1, then equation (2) implies a relation between the timescales in the two systems. The second system will evolve identically to the first system, on a timescale given by

$$\tau_1 = \tau \frac{h_1}{h}\sqrt{\frac{\tilde{p}/\tilde{\rho}}{\tilde{p}_1/\tilde{\rho}_1}}\,. \tag{5}$$

Here we have replaced t in equation (2) with a characteristic value, τ. The timescale τ can be any physically meaningful timescale, such as the characteristic time for h to change, a shock crossing time, or an instability growth time.

Provided that the similarity conditions are satisfied, an experiment done in system (r, ρ, p, t) or in (r_1, ρ_1, p_1, t_1) is probing identically the same physics, described by equations (1). This is independent of whether the system experiences strong or weak shocks, decompresses, develops unstable structures, enters the nonlinear regime, or becomes turbulent. Note in particular that we have made no assumptions with regard to the possible role of compressibility in the development of these systems. In addition,. within the limits discussed in § 2.3, phenomena that occur on some fraction of the scale h or τ in one system map to the same fraction of h_1 or τ_1 in another system.

Consider now the important special situation of system driven by a strong external source of momentum and energy. One can, for example, think of a piston that is pushed into the matter. By "strong" we mean that the source drives motions with velocities considerably exceeding the initial sound velocity. This is a typical situation both in supernovae and in the laser experiments on supernova hydrodynamics.

In the case of strongly driven systems, the similarity criteria become greatly simplified. What matters is only similar initial spatial distribution of density and similar time dependence of the drive. The specific values of the density $\tilde{\rho}$, of the initial scale h, or of the drive velocity v_d (aside from the requirement that it should be large) do not matter, because the states behind the shock are governed by strong shock relationships and, for systems with the same γ, automatically satisfy the conditions of Euler similarity. Figure 1 illustrates the relation described by equation (4) for two of the systems discussed below.

In a strongly driven system there exists an obvious expression for the timescale,

$$\tau \sim \frac{h}{v_d}\,, \tag{6}$$

because there is only one parameter of the dimension of velocity in the problem, the drive velocity v_d, unlike the general case described by equations (3), where there are two parameters, $\tilde{v}$ and the initial sound speed. The pressure in the strong-drive case scales as

$$\tilde{p} \sim \tilde{\rho}\tilde{v}_d^2\,. \tag{7}$$

To sum up the strong-drive discussion: the two systems experiencing a strong drive evolve similarly if the following two conditions are satisfied: (*a*) initial density distributions are similar (including any density nonuniformities) and, (*b*) the temporal dependence of the drives is similar.

To get the maximum benefit from the similarity just described, it is advisable to arrange the simulation experiment to have the same adiabatic relation between p and ρ as plasma in a real object. The adiabatic index should be approximately equal to 4/3 for cases in which the radiation pressure dominates and 5/3 in simulations of fully ionized regions with a small radiation pressure. Fortunately, the system under consideration is "structurally stable" with respect to moderate variations of the equation of state (the type of hydrodynamic equations is not changed by these variations). In other words, the moderate variations of the equation of state should not bring about any qualitatively new phenomena. In this sense, the difference of the adiabatic index from the best-fit value, as well as modest deviation from the polytropic law, are admissible. What would be inadmissible, for example, would be a situation where the equation of state contained steep dependencies on p and ρ, such as might occur at a phase transition. But in the range of temperatures ($\sim$5–25 eV) and pressures ($\sim$1–5 Mbar) involved in simulation experiments using sufficiently low-Z materials, such "special" features are absent.

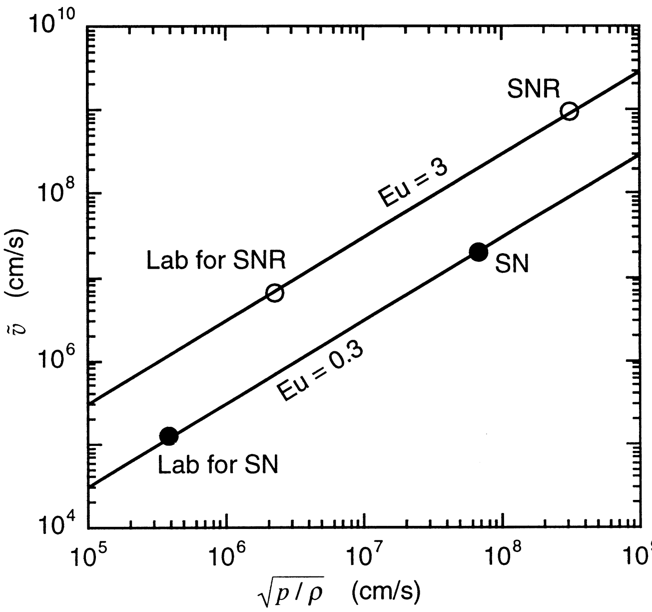

FIG. 1.—Identical hydrodynamic systems, when evaluated in the same way, have equal values of the parameter $\tilde{v}(\tilde{\rho}/\tilde{p})^{1/2}$ (Euler number, Eu). Here we show lines of constant $\tilde{v}(\tilde{\rho}/\tilde{p})^{1/2}$ for some systems discussed here (Tables 1–4), on axes of system velocity ($\tilde{v}$ or v_d) and a quasi-sonic velocity, $(p/\rho)^{1/2}$. The specific parameters for the systems are also plotted. The upper curve corresponds to $\tilde{v}(\tilde{\rho}/\tilde{p})^{1/2} = 3$; the lower curve corresponds to $\tilde{v}(\tilde{\rho}/\tilde{p})^{1/2} = 0.3$.

2.2. *Underlying Assumptions*

The Euler equations describe systems that behave as hydrodynamic fluids and in which heat transport and viscosity are unimportant. We assume without further discussion that gravitational forces are negligible in comparison with the accelerations caused by the SN explosion. We also assume that any planar experiment is intended only to model a local region of an evolving SN or SNR, for a limited time, so that the effects of spherical divergence are not significant. We organize our discussion of the validity criteria for Euler's equations into four parts. For Euler's equations to be valid, (1) the system needs to be "collisional"; (2) energy flow by particle heat conduction needs to be negligible; (3) energy flow by radiation flux needs to be negligible; and, finally, (4) viscous dissipation needs to be insignificant. We examine these assumptions in turn here.

2.2.1. *Collisionality*

The assumption of fluidlike behavior requires that the particles in the system be localized. The localization must occur on spatial scales that are small compared to h, the characteristic spatial scale of the system. Two ways to achieve this are through magnetic fields or through collisions. One thus requires either $r_{\mathrm{Li}}/h \ll 1$ or $l_c/h \ll 1$, where

$r_{\rm Li}$ is the ion Larmor radius and l_c is the collisional mean free path. Since the energy represented by the driving velocity is never completely thermalized, v_d and the corresponding energy can be used as an upper limit on the thermal velocity of the shocked matter. In this case the localization condition becomes either

$$\frac{r_{\rm Li}}{h} \approx 10^{-4} \frac{v_d({\rm cm\ s^{-1}})}{B({\rm G})h({\rm cm})} \ll 1 , \quad (8)$$

or

$$\frac{l_c}{h} \cong 3 \times 10^{13} \frac{T({\rm eV})^2}{\Lambda h n_i} \approx 8 \times 10^{-12} \frac{v_d^4}{\Lambda h n_i} \ll 1 , \quad (9)$$

in which the units are Gaussian cgs, n_i is the ion density, Λ is the Coulomb logarithm, $T \approx m v_d{}^2/2$, and we have used the ion-ion mean free path from Braginski (1965) for hydrogen. Differences among species of ions and electrons are significant only if the condition is marginal. We note that Λ does vary for the range of potential environments discussed here, but can be taken to be 6 to within a factor of a few.

The issues of localization along the magnetic field is a significant uncertainty here, and in all subsequent discussions of magnetized parameters. Indeed, if the magnetic field were of a regular structure and if plasma microfluctuations were completely absent, then the system would behave anisotropically and the hydrodynamic equations would not apply. However, solar system studies, laboratory experiments, and fundamental reasoning all would suggest that both magnetic entanglement and microscopic fluctuations will be present. One way to state the resulting requirement is that either magnetic entanglement or microfluctuations must localize the system along field lines in a distance small compared with $h/r_{\rm Li}$ gydroradii. In the young SNR case of § 3.2 below, this number is so large that there is no doubt that the system will behave hydrodynamically. The ring-collision case of § 3.3 is more complicated, however.

2.2.2. *Heat Conduction*

The dimensionless parameter that characterizes the role of diffusive heat transport by particles is the Peclet number (Book 1987), which corresponds to the ratio of heat convection to heat conduction. For the hydrodynamic equations (1) to be valid requires that the Peclet number be large,

$$\mathrm{Pe} = \frac{hv}{\chi} \gg 1 , \quad (10)$$

that is, convective (hydrodynamic) transport needs to dominate conduction. Here χ is the thermal diffusivity for electrons, which makes the main contribution to the heat conduction. The thermal diffusivity depends upon whether the electrons are magnetized, and it can be taken to be the minimum of the unmagnetized and magnetized values. The electrons may not be magnetized in the SN and are not in the laboratory experiments now underway, but are definitely magnetized in the developing SNR. For unmagnetized electrons, χ, based on (Braginski 1965), is

$$\chi({\rm cm^2\ s^{-1}}) = 2 \times 10^{21} \frac{[T({\rm eV})]^{5/2}}{\Lambda Z(Z+1) n_i({\rm cm^{-3}})} = 3.3 \times 10^{-3} \frac{A[T({\rm eV})]^{5/2}}{\Lambda Z(Z+1)\rho({\rm g\ cm^{-3}})} . \quad (11)$$

The numerical coefficient (which varies somewhat with Z) corresponds to $Z = 2$.

For magnetized electrons, evaluation of χ is more complicated. The possible presence of plasma microfluctuations can strongly inhibit parallel heat flux. The inhibition may also be produced by a stochastization of the magnetic field lines. If the characteristic length at which the magnetic field line changes its direction by $\sim \pi/2$ is $l_{\rm magn}$, this length will serve as a step size in a random walk that determines electron heat transport. The corresponding estimate for χ reads as

$$\chi \sim l_{\rm magn} v_{\rm Te} , \quad (12)$$

where $v_{\rm Te}$ is the thermal velocity of the electrons, defined here as $(2T/m)^{1/2}$, with m being the electron mass. If the magnetic field entanglement is caused by instabilities of the fire-hose type (e.g., Schmidt, 1966), then a natural scale of $l_{\rm magn}$ is the ion Larmor radius $r_{\rm Li}$. If entanglement is produced by larger scale turbulent plasma motion, then $l_{\rm magn}$ can considerably exceed $r_{\rm Li}$. To reflect the presence of this uncertainty, we introduce a parameter

$$\alpha \equiv l_{\rm magn}/r_{\rm Li} > 1 \quad (13)$$

and write the estimate for the electron thermal diffusivity as

$$\chi \sim \alpha v_{\rm Te} r_{\rm Li} . \quad (14)$$

In practical units, one has

$$\chi({\rm cm^2\ s^{-1}}) = 8.6 \times 10^9 \alpha \frac{\sqrt{A}}{Z} \frac{T({\rm eV})}{B({\rm G})} . \quad (15)$$

Here again, the exact structure of the magnetic field and the exact level of microfluctuations will determine the heat transport rate along B. So long as Pe is very large, this uncertainty will not be significant.

Note that, although the magnetic field can be high enough to affect thermal conductivity, its pressure $B^2/8\pi$ is typically very small compared to the plasma pressure in the SN (Chevalier & Luo, 1994; Jun & Norman, 1996). Therefore, one can use the Euler equations without magnetic stresses to describe the SN hydrodynamics.

2.2.3. *Radiation Flux*

Energy fluxes carried by radiation must be small compared with the hydrodynamic energy fluxes. The corresponding condition depends upon the system properties, and there are two cases. (*a*) If the mean free path of the photons, $\bar{l}$, is much less than h, then one can evaluate the radiation contribution to thermal diffusivity, χ_γ, and establish a corresponding Peclet number, Pe_γ, which must be large. In some cases (especially in the dense laboratory plasma with the temperature of the order of a few electron volts), it is difficult to evaluate χ_γ without very time-consuming numerical simulations. Then, an upper estimate of the radiative heat flux, the blackbody radiation flux (σT^4), may be sufficient to demonstrate that the radiative losses are negligible. (*b*) If $\bar{l} \gg h$, then the radiative cooling time is that corresponding to optically thin emission, $\tau_{\rm thin}$. In this case, one requires $\tau_{\rm thin}/\tau \gg 1$, where τ is a characteristic hydrodynamic time.

In the case of a hot fully ionized plasma of the SN interior, the mean free path of the photons can be taken to be min ($\bar{l}_{\rm brems}$, $\bar{l}_{\rm Thomson}$), where the mean free path due to inverse bremsstrahlung, averaged over a Planckian distribution of photons (the Rosseland mean), in a fully ionized plasma is (see Book 1987, p. 57, eq. [31])

$$\bar{l}_{\rm brems}({\rm cm}) = 1.7 \times 10^{37} \frac{[T({\rm eV})]^{7/2}}{Z^3[n_i({\rm cm}^{-3})]^2}$$
$$= 4.6 \times 10^{-11} \frac{A^2[T({\rm eV})]^{7/2}}{Z^3[\rho({\rm g\ cm}^{-3})]^2} , \quad (16)$$

in which T is the temperature and A, Z, and n_i are the atomic weight, charge, and density, respectively, of the ions. The mean free path $\bar{l}_{\rm Thomson}$ with respect to Compton scattering is

$$\bar{l}_{\rm Compton}({\rm cm}) = 1/[n_e({\rm cm}^{-3})\sigma_{\rm T}({\rm cm}^2)] = 2.5A/Z\rho({\rm g\ cm}^{-3}) , \quad (17)$$

where $\sigma_T = (8\pi/3)r_e^2 = 6.6 \times 10^{-25}$ cm^2 is the Thomson cross section, n_e is the electron density, and ρ is the mass density.

We now can state the limits for the two cases just described. For case *a*, an expression for χ_γ is

$$\chi_\gamma = \kappa_\gamma/c_v , \quad (18)$$

where κ_γ is the radiative thermal conductivity,

$$\kappa_\gamma = \tfrac{16}{3}\bar{l}\sigma T^3 \quad (19)$$

(e.g., Zeldovich & Raizer, 1966), and c_V is the thermal capacity per unit volume,

$$c_V = \frac{16\sigma T^3}{c} + \frac{3(Z+1)n_i}{2} . \quad (20)$$

The first term here represents the thermal capacity of radiation, whereas the second term represents the thermal capacity of electrons and ions. The first term is dominating in the case where the radiation pressure is higher than the plasma pressure, and vice versa. The condition of a negligible radiative heat flux is the condition that the Peclet number evaluated with the radiative thermal diffusivity χ_γ be large,

$$\mathrm{Pe}_\gamma \equiv hv/\chi_\gamma \gg 1 . \quad (21)$$

In the situations where it is difficult to evaluate the photon mean free path, the aforementioned upper (blackbody) estimate for the radiative heat fluxes can be used to provide a *sufficient* condition for radiative heat transport to be negligible. The arguments here go like this: the maximum possible energy loss from the surface of the plasma slab (per unit area, per unit time) is that corresponding to the blackbody radiation at the temperature inside the slab, $2\sigma T^4$; on the other hand, the plasma energy content per unit area of the slab surface is $(3/2)h(n_e + n_i)T$. Dividing the second by the first, one finds a lower limit for the radiation cooling time, $\tau_{\rm BB} = (3/2)(Z+1)n_i Th/(2\sigma T^4)$, or

$$\tau_{\rm BB}(s) = 1.2 \times 10^{-24} \frac{(Z+1)n_i({\rm cm}^{-3})h({\rm cm})}{[T({\rm eV})]^3}$$
$$= 0.7 \frac{(Z+1)\rho_i({\rm g\ cm}^{-3})h({\rm cm})}{A[T({\rm eV})]^3} . \quad (22)$$

A sufficient condition that the radiative losses are negligible is that

$$\tau_{\rm BB} \gg \tau , \quad (23)$$

where τ is a characteristic hydrodynamical time.

For the optically thin plasma (case *b*), the cooling is due to bremsstrahlung, and at some temperatures to line radiation. After finding the cooling time by dividing the energy density by the radiated power per unit volume, we obtain

$$\tau_{\rm thin}(s) = 2.4 \times 10^{-12} \frac{(Z+1)T({\rm eV})}{Zn_i({\rm cm}^{-3})\Lambda_N}$$
$$= 4.0 \times 10^{-36} \frac{A(Z+1)T({\rm eV})}{Z\rho_i({\rm g\ cm}^{-3})\Lambda_N} \gg \tau , \quad (24)$$

in which Λ_N is the normalized cooling rate (Sutherland & Dopita 1993), in ergs cm^3 sm^{-1}. For temperatures above a few keV, the cooling is due to bremsstrahlung, for which (Book 1987) the cooling rate is $\Lambda_N = 1.7 \times 10^{-25} Z_{\rm eff}^2 T({\rm eV})^{1/2}$, in which $Z_{\rm eff}^2$ is the usual weighted average of Z^2. At lower temperatures the line radiation can decrease $\tau_{\rm thin}$ by up to about 2 orders of magnitude compared to bremsstrahlung. Optically thin regions having initial shocked temperatures from 30 eV to about 3 keV can potentially be affected. This is apparently important for the ring collision, as discussed in § 3.3. Our discussion of heat conduction by photons as a limit on the applicability of the Euler equations is now complete.

2.2.4. *Viscosity*

In seeking systems to which the Euler equations apply, we also require that viscous effects be unimportant. This amounts to a condition on the Reynolds number, Re, which corresponds to the ratio of inertial force to viscous force (Book 1987). The condition is

$$\mathrm{Re} = \frac{hv}{\nu} \gg 1 , \quad (25)$$

in which ν is the kinematic viscosity. All sources of viscosity must be added. The photon viscosity is (Jeans 1926a, 1926b; Thomas 1930)

$$\nu_{\rm rad}({\rm cm}^2\ {\rm s}^{-1}) \sim \frac{\bar{l}c\sigma T^4}{\rho c^3} \approx 3 \times 10^{-9} \frac{A}{Z} \frac{[T({\rm eV})]^4}{[\rho({\rm g\ cm}^{-3})]^2} . \quad (26)$$

The particle viscosity again depends on the magnetization, and one should take the smaller of the following two values. In the collisional limit (insignificant magnetic field), the viscosity of the ions dominates that of the electrons for Z below about 6 and is

$$\nu_i({\rm cm}^2\ {\rm s}^{-1}) = 2 \times 10^{19} \frac{[T({\rm eV})]^{5/2}}{\Lambda\sqrt{A}Z^4 n_i({\rm cm}^{-3})}$$
$$= 3.3 \times 10^{-5} \frac{\sqrt{A}[T({\rm eV})]^{5/2}}{\Lambda Z^4 \rho_i({\rm g\ cm}^{-3})} . \quad (27)$$

In the magnetized case, the ion viscosity can be estimated as $\alpha r_{\rm Li} v_{\rm ti}$, in which α is a coefficient greater than 1 defined by equation (13), and v_{ti} is the ion thermal velocity, defined as $(2/M)^{1/2}$, in which M is the ion mass. In practical units, this is

$$v_i(\mathrm{cm}^2\ \mathrm{s}^{-1}) = 2 \times 10^8\ \frac{\alpha T(\mathrm{eV})}{ZB(\mathrm{G})}\ . \tag{28}$$

This again amounts to assuming that the field entanglement localizes the particles on the scale of αr_{Li}, and the same considerations regarding transport along B that were discussed previously apply here. So long as Re is very large, the uncertainty here is also not significant.

2.3. *At What Spatial Scales Does the Euler Similarity Break Down?*

We emphasize again that the hydrodynamic similarity between laboratory laser experiments and supernovae, expressed by equations (1)–(3), holds even when the system reaches a deeply nonlinear stage in its evolution. The limit of applicability of this similarity is set by the validity of Euler's equations as an adequate description of the hydrodynamics. These equations break down at spatial scales much less than the global scale $h \equiv \rho/|\nabla\rho|$, where dissipative processes become important. For example, small-scale Rayleigh-Taylor (RT) perturbations of characteristic scale length $\bar{\lambda} \ll h$ (where $\bar{\lambda} = 1/k = \lambda/2\pi$) have growth rates (see, e.g., a survey by Kilkenny et al. 1994) $\gamma_{\mathrm{RT}} \sim (g/h)^{1/2} \sim v/h$, where we use an estimate $g \sim v^2/h$ for the effective gravitational acceleration g. The characteristic time for viscous dissipation (Landau & Lifshitz 1987) at spatial scales $\sim\bar{\lambda}$ is $\tau_{\mathrm{vis}} \sim \bar{\lambda}^2/\nu$ where ν is the kinematic viscosity (§ 2.2.4). Viscosity becomes important for these perturbations when $\tau_{\mathrm{vis}} < 1/\gamma_{\mathrm{RT}}$, meaning $\bar{\lambda}^2/\nu < h/v$ or, equivalently, at

$$\bar{\lambda}/h < \mathrm{Re}^{-1/2}\ . \tag{29}$$

Analogously, the heat conduction effects become important at

$$\bar{\lambda}/h < \mathrm{Pe}^{-1/2}\ . \tag{30}$$

If, on a background density variation of scale length h, there exists a density discontinuity, the RT growth rate scales as $(g/\bar{\lambda})^{1/2}$; in this case, the exponents on the right-hand sides of equations (29) and (30) should be replaced by $-\frac{2}{3}$ (Chandrasekhar 1961). Note that Chandrasekhar does not introduce the estimate $g \sim v^2/h$ for the effective gravitational acceleration into his analysis; therefore, his estimates do not explicitly contain the Reynolds number.

The possible development of turbulence due to the Kelvin-Helmholtz (KH) instability leads to the generation of small-scale vortices; the viscous effects become important when the size of these vortices reaches the level (see Landau & Lifshitz 1987)

$$\bar{\lambda}/h < (\mathrm{Re}/\mathrm{Re}_{\mathrm{crit}})^{-3/4}\ , \tag{31}$$

where $\mathrm{Re}_{\mathrm{crit}} \sim 10^3$ is the critical Reynolds number that marks the onset of the KH instability in sheared flow. Viscous dissipation and the specific value of the Reynolds number do not affect phenomena occurring at the scale exceeding expression (31).

Whether the small scales defined by equations (29)–(31) are of importance depends on the specifics of the problem. For example, the scales in equation (31) may be important in causing "molecular" mixing of the components and may affect reaction rates, such as the thermonuclear burn of a Type I supernova. But such short-scale features may be unimportant for the dynamic evolution of the system at larger scales. In particular, they do not affect the simulations of the global properties of the system, such as, for example, the arrival time of the first RT spikes at the surface of a star.

3. SPECIFIC SIMULATION EXPERIMENTS

In this section, we apply the results of § 2 to three specific examples. This involves first specifying the parameters of an astrophysical system and the corresponding laboratory system, and then deriving the measures of similarity and of validity discussed in § 2. We discuss three cases related to SN 1987A: the exploding star, the young SNR, and the ring collision. After that, we discuss the possibility of simulating the objects where radiation plays a more significant role than in SN 1987A.

3.1. *The Exploding Star*

We focus on the most hydrodynamically (Rayleigh-Taylor) unstable region of the exploding star, the He-H interface, using parameters that correspond to models of SN 1987A at a time of about 2000 s after the core collapse. The motivation for studying this issue is the outward thrust of material under the influence of hydrodynamic instabilities, which allows the core of the star to penetrate toward the surface. Details of experiments performed with the Nova laser can be found in Kane et al. (1997) and Remington et al. 1997a, 1997b.

The specified parameters for the two cases are given in Table 1, and are based on numerical simulations by Kane et al. (1997), as illustrated in Figure 2. Other groups have also modeled the SN explosion (Hillebrandt et al. 1987; Shigeyama, Nomoto, & Hashimoto 1988; Woosley, Pinto, & Ensman 1988; Arnett, Fryxell, & Muller 1989; Muller et al. 1989). Figure 2 shows the density and pressure distribution at the time $t = 2000$ s for the SN 1997A case and $t = 20$ ns for the experiment. The spatial scale h listed in Table 1 was chosen to be the width of the density profile at the half-maximum level. We define $\tilde{v} = \dot{h}$ as a reference velocity (the scaling factor in eq. [3]), where $\dot{h}$ is the time derivative of h. The other parameters in the table are evaluated midway between the two jumps in density. The electron-ion equili-

TABLE 1

SPECIFIED PARAMETERS OF SN He PLASMA AT 2000 s AND CORRESPONDING Cu PLASMA IN THE EXPERIMENT AT 20 ns

Item	Symbol	Value in SN	Value in Laboratory
Scale height (cm)..........	h	9.0×10^{10}	0.0053
Velocity (km s^{-1}).........	$\tilde{v}$	200	1.3
Density (g cm^{-3})	$\tilde{\rho}$	0.0075	4.2
Pressure (dyn cm^{-2})......	$\tilde{p}$	3.5×10^{13}	6.0×10^{11}
Temperature (eV)	T	900	3.8
Z_i	Z	2.0	1.5
A	A	4.0	64
Ion density (cm^{-3})........	n_i	1.1×10^{21}	4.0×10^{22}

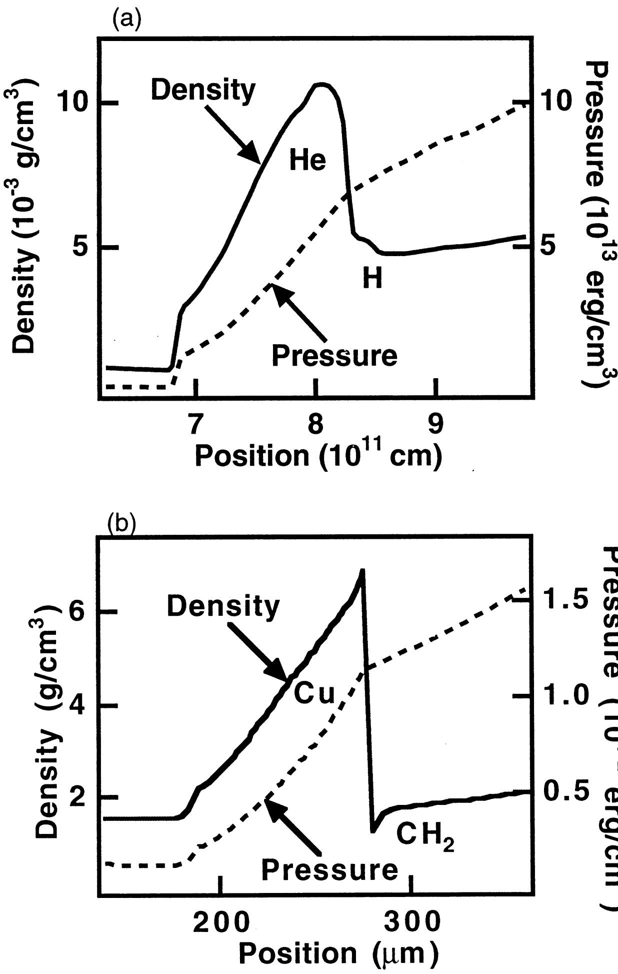

FIG. 2.—Hydrodynamic solutions for the SN and the laboratory experiment: spatial profiles of the pressure and density for the SN at 2000 s and the laboratory experiment at 20 ns; note the difference of the horizontal and vertical scales in the two cases.

bration time is short compared to hydrodynamic timescales, so the single temperature, T, can characterize the plasma.

The He and H layers in the SN are at a temperature of nearly 1 keV, and the plasma is fully ionized. The pressure is dominated by radiation, as illustrated below. The radiation pressure is equal to

$$P_{\rm rad} = 4\sigma T^4/3c \, , \tag{32}$$

where σ is the Stefan-Boltzmann constant and c is the speed of light. In "practical" units,

$$P_{\rm rad}({\rm ergs\ cm^{-3}}) = 46[T({\rm eV})]^4 \, . \tag{33}$$

For a temperature of $T = 900$ eV, this gives $P_{\rm rad} = 3 \times 10^{13}$ ergs cm^{-3} = 30 Mbar. For comparison, the particle pressure of the fully ionized helium plasma is equal to

$$P = 3n_{\rm He} T \, , \tag{34}$$

where $n_{\rm He}$ is the number density of He ions. In "practical" units,

$$n_{\rm He}({\rm cm^{-3}}) = 1.5 \times 10^{23} \rho({\rm g\ cm^{-3}}) \, , \tag{35a}$$

$$p({\rm ergs\ cm^{-3}}) = 7.2 \times 10^{11} \rho({\rm g\ cm^{-3}}) T({\rm eV}) \, . \tag{35b}$$

For $\rho = 7.5 \times 10^{-3}$ g cm^{-3}, $T = 900$ eV, from Table 1, one has $p = 4.9 \times 10^{12}$ ergs cm^{-3} = 4.9 Mbar, a factor of 6 less than the radiation pressure.

Table 2 shows the derived parameters, based on the discussion in § 2, for these systems. The geometric profiles for density and pressure are similar for the SN and the laser experiment, as illustrated in Figure 2. Similarity criteria specified by equation (4) are met to within $\sim$10%. Hence, the laser experiment and the SN are hydrodynamically equivalent, provided the four conditions discussed in § 2 are satisfied. This is the case, as the entries in Table 2 show. The localization condition (eq. [9]) is satisfied; that is, both fluids can be treated hydrodynamically. The Peclet number for electron heat transport (eq. [10]) is large in both cases, as is the Reynolds number. Although the Reynolds number is smaller in the laboratory experiment than in the SN, at a value $\sim 10^6$, it remains many orders of magnitude higher than a typical "critical" Reynolds number corresponding to the onset of instability in a sheared flow (${\rm Re_{crit}} \sim 10^3$). Therefore, it is clear that viscous effects will not alter the plasma behavior in the laboratory experiment. In the SN case, the viscosity is dominated by the photon viscosity (see eq. [26]) and also is negligible.

Note that the states we are comparing in a supernova and in the laser experiment have been reached long after the passage of a strong shock. The fact that the states produced by this strong shock in the SN and the laboratory experiment obey the Euler similarity shows that the initial state of the experimental package and the time dependence of the drive have been chosen correctly in the laser experiment.

The entries concerning radiation in Table 2 show that radiation does not significantly impact the hydrodynamics. For the SN case, radiation dominates the heat transport, so the condition (that radiation does not significantly impact the hydrodynamics) is that ${\rm Pe}_\gamma$ for photons must be large, which, at a value of $\sim 10^5$, it is. For the laboratory case, bremsstrahlung and line transport set the diffusive scale for the radiation transport. It is difficult to make quantitative statements with regard to χ_γ in such a situation, in particular because of the sensitivity of the results to the presence of dopants. Therefore, we resort to the estimate of the radiative fluxes from above, as described by equations (22) and (23), and find that the blackbody cooling time (the lower estimate for the cooling time) is, indeed, much longer than the characteristic hydrodynamic time.

We can compare the timescales in the two cases using equation (5). This shows that 1.4 ns in the laboratory experiment corresponds to 130 s in the SN explosion. We can also compare the Rayleigh-Taylor parameters in these two cases. We take v to be the velocity of the point of maximum density. Multiplying the Rayleigh-Taylor growth rate for the perturbation with $k \sim 2/h$, $\gamma_{\rm RT} \sim (2\dot{v}/h)^{1/2}$, by the characteristic time $\tau = h/\dot{h}$, gives the number Γ of (linear regime) e-foldings that occur within this time interval. Thus we obtain $\Gamma = (2\dot{v}h/\dot{h}^2)^{1/2}$ in this case. The values of this parameter for the two systems at $t = 2000$ s and 20 ns are approximately 2.5—close to each other.

For the next $\sim$500 s (in the SN) after the parameters in Table 2 are defined, the radius of the interface in the SN changes by 40%, meaning that within this time interval effects of spherical geometry are not large. Finally, any minor differences in the equations of state cannot cause strong changes in the overall evolution of the system. Therefore, the hydrodynamic evolution of the two systems

TABLE 2

Derived Parameters of SN He Plasma at 2000 s and Corresponding Cu Plasma in the Experiment at 20 ns

Item	Symbol	Value in SN	Value in Laboratory
Hydrodynamics:			
Eq. (4)	$\tilde{v}\sqrt{\tilde{\rho}/\tilde{p}}$	0.29	0.33
Localization	l_c/h	4×10^{-14}	1.1×10^{-8}
Particulate heat transport:			
Thermal diffusivity (e^-) (cm^2 s^{-1})	χ	1.2×10^6	0.38
Peclet number (e^-)	Pe	1.5×10^{12}	1.8×10^3
Momentum transport:			
Total viscosity (cm^2 s^{-1})	ν	7.0×10^7	3.5×10^{-4}
Reynolds number	Re	2.6×10^{10}	1.9×10^6
Radiation:			
Collision mfp (cm)	$\bar{l}_{\rm brems}$	37,000	3.4×10^{-7}
Compton mfp (cm)	$\bar{l}_{\rm Compton}$	680	26
Photon diffusivity (cm^2 s^{-1})	χ	6.8×10^{12}	...
Photon Peclet number	Pe$_\gamma$	2.6×10^5	...
Blackbody cooling time	$\tau_{\rm BB}/\tau$	...	580
Coulomb logarithm	Λ	6	1

over this limited interval of time is indeed similar, including the evolution of the unstable perturbations.

3.2. *The Young SNR*

We now apply a similar analysis to the case of a young SNR. The ejecta from the SN drive a blast wave out through the ambient circumstellar matter (CSM). In the young phase of the SNR, this produces a structure including a forward shock, shocked CSM, a contact discontinuity between ejecta and CSM, shocked ejecta, and a reverse shock. We show in Table 3 parameters appropriate to the shocked ejecta in SN 1987A at about 13 yr and in the plasma of the laser experiment now in progress at about 8 ns. The values for SN 1987A are based on Suzuki, Shigeyama, & Nomoto (1993), while those for the lab experiment are based on Drake et al. (1998).

The spatial scale height shown in Table 3 is the distance from the reverse shock to the contact discontinuity in the two cases. For the characteristic velocity $\tilde{v}$ we have chosen the velocity of the contact discontinuity. The other parameters were evaluated in the dense region of the shocked ejecta. It is believed that the magnetic field in SNRs is in the range 10^{-5}–10^{-4} G (Ellison & Reynolds 1991). The magnetic field for SN 1987A is based on Kirk & Wassman (1992) and Duffy, Ball, & Kirk (1995). There is uncertainty associated with the use of a single temperature in the SNR, as the electrons and ions are not rapidly equilibrated by collisions. (They are very rapidly equilibrated in the experiment.) The ion temperature is determined by the hydrodynamics, but the electron temperature might be smaller than T. This uncertainty is unimportant here, however, as it is magnetization rather than collisions that determines the electron heat transport in the SNR.

TABLE 3

Characteristic Parameters of Shocked Ejecta for Young SNR at 13 yr and Corresponding Laboratory Experiment at 8 ns

Item	Symbol	Value in SNR	Value in Laboratory
Scale height (cm)	h	3.0×10^{16}	0.01
Drive velocity (km s^{-1})	v_d	9500	65
Density (g cm^{-3})	$\tilde{\rho}$	1.0×10^{-22}	0.6
Pressure (dyn cm^{-2})	$\tilde{p}$	1.0×10^{-5}	3.0×10^{12}
Temperature (eV)	T	3.0×10^4	15
Z	Z	1.2	2
A	A	1.6	6.5
Ion density (cm^{-3})	n_i	40	5.5×10^{22}
Magnetic field (G)	B	1.0×10^{-4}	N/A

Table 4 shows the derived parameters, based on the discussion in § 2, for these two systems. A similarity criterion (eq. [4]) holds with a good accuracy. [Note that the parameter $\tilde{v}(\tilde{\rho}/\tilde{p})^{1/2}$ is noticeably larger than 1 because in this case we have chosen a different (compared to § 3.1) measure of the velocity: the velocity of a contact discontinuity.] In addition, the two systems have similar spatial profiles (Drake et al. 1998), and the driving velocity varies little in either case over the period for which comparisons are valid (years for the SNR and nanoseconds for the laser experiment). Thus, the basic conditions for Euler similarity are met, and the laboratory system is a well-scaled hydrodynamic simulation of the SNR.

The four conditions of § 2 are met for both the SNR and the laboratory experiment. Both plasmas behave as hydrodynamic fluids (see eqs. [8] and [9])—the SNR because it is magnetized ($r_{\rm Li}/h \ll 1$), and the experiment because of collisions ($l_c/h \ll 1$). Thermal heat conduction is small in both systems, as indicated by the large Peclet numbers. Both systems also have large Reynolds numbers. For both heat conduction and viscosity, the magnetic field is essential in determining the behavior of the SNR. Radiation cooling is small in both cases, although the laser experiment is in the optically thick regime whereas the SNR is in the optically thin regime. We thus conclude that the hydrodynamic behavior of the laboratory system is directly relevant to that of the remnant of SN 1987A.

For this strongly driven case, the timescales are implied by equation (6). A timescale of roughly 1 year in the SNR corresponds to a timescale of 1.5 ns in the laboratory. The

TABLE 4

DERIVED PARAMETERS OF SHOCKED EJECTA FOR YOUNG SNR AT 13 yr AND CORRESPONDING LABORATORY EXPERIMENT AT 8 ns

Item	Symbol	Value in SNR	Value in Laboratory
Hydrodynamics:			
Eq. (4)	$\tilde{v}\sqrt{\tilde{\rho}/\tilde{p}}$	3.0	2.9
Strong drive timescale (s)	h/v_d	3×10^7	1.5×10^{-9}
Localization	$r_{\rm Li}/h$	3×10^{-8}	N/A
Localization	l_c/h	N/A	1×10^{-6}
Particulate heat transport:			
Thermal diffusivity (e^-) (cm^2 s^{-1})	χ	3×10^{18}	5
Peclet number (e^-)	Pe	10^7	1.2×10^4
Momentum transport:			
Collisional viscosity (cm^2 s^{-1})	ν_i	N/A	9×10^{-3}
Photon viscosity (cm^2 s^{-1})	$\nu_{\rm rad}$	N/A	10^{-3}
Magnetized viscosity (cm^2 s^{-1})	υ_i	5×10^{16}	N/A
Reynolds number	Re	6×10^8	7×10^6
Radiation:			
Collision mfp (cm)	$\bar{l}_{\rm brems}$	2.2×10^{49}	9.1×10^{-6}
Compton mfp (cm)	$\bar{l}_{\rm Compton}$	2.5×10^{22}	14
Blackbody cooling time	$\tau_{\rm BB}/\tau$	N/A	380
Optically thin cooling	$\tau_{\rm thin}/\tau$	2.8×10^6	N/A
Coulomb logarithm	Λ	32	1

upper limit for the time interval over which the evolution of the two systems is similar is not constrained, except by the limitations implied in the comparison of the spherical SNR to a planar experiment.

3.3. *The Ring Collision*

There is yet no experiment that reproduces all the relevant features of the ring collision in SN 1987A, which turns out to be a more complicated system. In the experiment of § 3.2, simulating the young SNR, the blast wave does impact dense material, producing a collision between the ejecta-driven structure and this higher density material in planar geometry. We discuss below the degree to which this is a good simulation of the actual ring-collision event. We further discuss some general issues relevant to the simulation of such ring collisions.

In the case of SN 1987A we base our discussion on the modeling of Borkowski, Blondin, & McCray (1997), with an assumed ring density of 32,000 amu cm^{-3} and CSM density of 6–100 amu cm^{-3} just inside the ring. We take $\tilde{v} = v_d$ to be the velocity of the shocked CSM that is incident on the ring, $\sim$10,000 km s^{-1}. The shocked CSM beside the ring takes about 3 yr to pass the ring. It takes another 3 yr to establish a well-defined bow shock that stops the ejecta incident on the ring and diverts it around the ring. In the modeling of Borkowski et al. (1997), there is then a quasi-steady period of order 10 yr before the destruction of the ring by hydrodynamic instabilities, including the KH instabilities along the sides, begins to affect the bow shock. In this model, it takes a few decades to completely destroy the ring.

The remaining defined parameters for this case are shown in Table 5.We take h to be 1 ring diameter, or $\sim 10^{17}$ cm (we assume here that the ring is a toroidal object and refer here to the minor diameter; the major diameter is $\sim 10^{18}$ cm). This is also the approximate distance between the forward shock in the CSM and the contact discontinuity between the CSM and the SN ejecta, at the time when the forward shock reaches the ring. We evaluate $\tilde{p}$ and $\tilde{\rho}$ in the shocked ring material. The magnetic field is taken to be 100 μG, as it was for the discussion of the young SNR in § 3.2.

The derived parameters are shown in Table 6, to set the stage for the discussion that follows. Because the ring is strongly driven by the incoming CSM, it is sensible to choose $\tilde{v} = v_d$ in this case, as we did. This results in a much larger value of the parameter $\tilde{v}(\tilde{\rho}/\tilde{p})^{1/2}$ than we found in the prior two cases, because the ring is so much denser than the CSM. This choice has the virtue that the strong drive timescale, of about 3 yr, does correspond to the timescales of the evolution of the system just described (a natural consequence of the time it takes the blast wave to pass the ring). For comparison, a model experiment with $h \sim 0.01$ cm $= 100$ μm and $v_d = 100$ km s^{-1} would have a natural timescale of 1 ns. One finds again that the system is well localized, and that the Peclet number and Reynolds number are large, although some caveats to this are discussed below.

In this case, in contrast to those above, radiation losses are significant. Because of the effects of line radiation, which were evaluated for a ratio of Fe abundance to H abundance of one-third solar, as is appropriate to SN 1987A, the initial

TABLE 5

SPECIFIED PARAMETERS OF SHOCKED PLASMA IN THE RING

Item	Symbol	Value in Ring
Scale height (cm)	h	1.0×10^{17}
Drive velocity (km s^{-1})	v_d	10,000
Density (g cm^{-3})	$\tilde{\rho}$	2.2×10^{-19}
Pressure (dyn cm^{-2})	$\tilde{p}$	3.5×10^{-5}
Temperature (eV)	T	170
Z	Z	1.2
A	A	1.6
Ion density (cm^{-3})	n_i	81,000
Magnetic field (G)	B	1.0×10^{-4}

TABLE 6

DERIVED PARAMETERS OF THE SHOCKED PLASMA IN THE RING

Item	Symbol	Value in Ring
Hydrodynamics:		
Eq. (4)	$\tilde{v}\sqrt{\tilde{\rho}/\tilde{p}}$	79
Strong drive timescale (s)	h/v_d	10^8
Localization	$\rho_{\rm Li}/h$	10^{-8}
Particulate heat transport:		
Thermal diffusivity (e^-) (cm^2 s^{-1})	χ	1.5×10^{16}
Peclet number (e^-)	Pe	7×10^9
Momentum transport:		
Collisional viscosity (cm^2 s^{-1})	ν_i	3.4×10^{19}
Photon viscosity (cm^2 s^{-1})	$\nu_{\rm rad}$	N/A
Magnetized viscosity (cm^2 s^{-1})	ν_i	3×10^{14}
Reynolds number	Re	3×10^{11}
Radiation:		
Collision mfp (cm)	$\bar{l}_{\rm brems}$	1×10^{35}
Compton mfp (cm)	$\bar{l}_{\rm Compton}$	1.6×10^{19}
Optically thin cooling	$\tau_{\rm thin}/\tau$	2.3
Coulomb logarithm	Λ	24

radiation cooling time is only 2.3 times the characteristic 3 yr hydrodynamic timescale. Thus, in the short run, radiation will not play a dominant role in the dynamics of the interaction of the heated ring plasma with the ejecta, and the Euler equations may apply. However, the shocked ring plasma is cool enough to be subject to the thermal cooling instability. This issue has been discussed by Borkowski et al. (1997), who concluded that the shocked zone in the ring will collapse after a few years. Of course, during the collapse, equations (1) will not describe the evolution, and an experiment intended to simulate this phase would also need to thermally collapse.

We now consider the degree to which the present experiment is relevant to the ring collision. The shock propagating in the CSM is a very strong shock. The pressure of the shocked CSM is much higher than the initial pressure of the ring material. Therefore, the drive is strong with respect to both the CSM and the ring material, and the hydrodynamic similarity between the real SNR and the simulating experiment requires only that the initial spatial density distribution is geometrically similar in both cases. The relation of the timescales, during this early phase of the evolution, will be determined by the temporal dependence of the drive. This is exemplified, for example, by the time it takes the shock reflected from the ring to reach the contact discontinuity in the SNR. One important feature of the published analyses of the ring collision is the effects of shock reverberation between the ring and the contact discontinuity in the SNR (Suzuki et al. 1993; Luo, McCray, & Slavin 1994; Masai & Nomoto 1994; Borkowski et al. 1997). The existing experiment may prove able to see this.

There is another caveat, however, in the comparison of laboratory experiments like that of § 3.2 with the actual ring collision. There is some chance that heat conduction from the shocked CSM into the ring will lead to additional ring heating and expansion. The Peclet number is large, so this should be at most a local effect, so long as the magnetic field is in fact entangled on the scale of the ion gydroradius, as assumed in our discussion of heat transport. However, there is such a large reservoir of energy in the blast wave, and there will be such steep temperature gradients across a narrow layer of magnetic field, that the electron thermal conductivity along the magnetic field lines might be large enough to transport heat into the ring at a significant rate. Therefore, the cold material of the ring may be heated not only via the shock heating produced by the forward shock in the dense material of the ring, but also by the electron thermal conductivity from the hot surrounding plasma. The surrounding plasma will be hot because it has been heated by the much faster shock in the low-density plasma outside the ring. This depends crucially on the magnitude of the electron thermal conductivity in the "braided" magnetic field near the forward shock. It is possible that the initially cold ring may be heated by electron conduction faster than the shock wave propagates through it. We believe this issue deserves further exploration, but this would be beyond the scope of the present paper.

3.4. *Radiative SNRs*

In case of SN 1987A, radiative losses are known to be insignificant before the ring collision because the density of the surrounding medium is quite low. In contrast, a more "typical" Type II SN, such as SN 1993J, in which a red supergiant star explodes, has a much higher ambient density. In these cases, the radiative losses are thought to be important (Chevalier 1982; Fransson 1984; Blondin, Fryxell, & Königl 1990; Chevalier & Fransson 1994; Chevalier 1997). To simulate such effects in the laboratory would require modified experiments, with higher shock-generated temperatures. In this section we identify plasma parameters for which the time of radiative cooling of the plasma is comparable to the hydrodynamic timescales.

We assume that such a laboratory plasma will be optically thin, or close to it, as is the case for the SNR. For radiative cooling to significantly affect the hydrodynamics, we require that the time $\tau_{\rm thin}$ of the radiative cooling be smaller than the characteristic gas dynamic time, h/s, where

$$s({\rm cm\ s^{-1}}) = 1.3 \times 10^6 \sqrt{\frac{(Z+1)T({\rm eV})}{A}} \tag{36}$$

is the sound speed for $\gamma = 5/3$. In other words, we require that radiation time be less than characteristic convection time. For the system to remain optically thin, we also require $h < \bar{l}_{\rm brems}$ (eq. [16]). The combined condition becomes

$$5.2 \times 10^{-30} \frac{\sqrt{A}(Z+1)^{3/2}[T({\rm eV})]^{3/2}}{Z\rho({\rm g\ cm^{-3}})\Lambda_N} < h({\rm cm}) < 4.6 \times 10^{-11} \frac{A^2[T({\rm eV})]^{7/2}}{Z^3[\rho({\rm g\ cm^{-3}})]^2}\,. \tag{37}$$

The cooling function, however, is more complicated for a high-density laboratory plasma than it is for an astrophysical plasma, as continuum lowering and three-body effects are important, while the distribution of ionization states and excited states may be both noncoronal and non-LTE. Here, for cooling, we show the result for bremsstrahlung and comment on the impact of line radiation on the cooling time. (And we again do not attempt to account for the impact of line radiation on the effective photon mean free path.) For a given h, A, and Z, equation (37) can be formulated as a pair of relations between T and ρ, with results shown in Figures 3 and 4 for two cases. Figure 3 shows results for $A = 1.6$, $Z = 1.2$, and $h = 10^{16}$ cm repre-

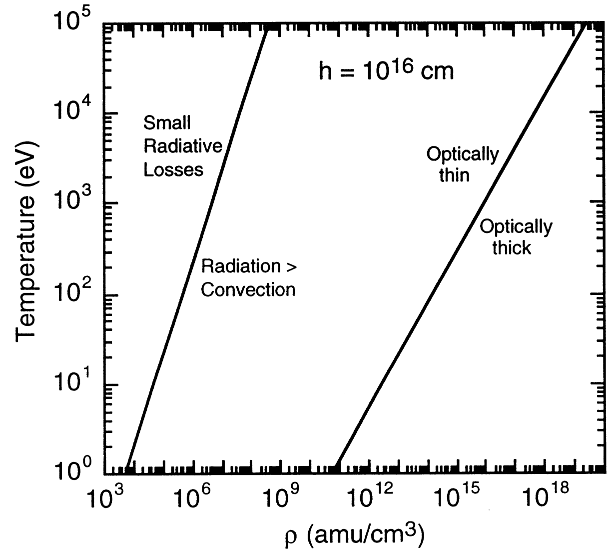

FIG. 3.—On the spatial scales appropriate to young SNRs, there is a large difference in density between the density at which radiation dominates over convection (*left line*) and the density at which the system, would become optically thick (*right line*). This figure is based on eq. (37).

sentative for the SNR. In this case there is a large range of densities for which radiative losses dominate over convection while the system remains optically thin. The impact of line radiation will be that the line on the left curves upward as the density decreases below 10^7 amu cm^{-3} and T drops below 3000 eV.

In contrast, Figure 4 shows that it is more difficult to satisfy equation (37) in the laboratory, showing results for $A = 12$, $Z = 6$, and $h = 0.01$ cm. For bremsstrahlung cooling, the temperature must exceed 100 eV before radiation losses can exceed convection in an optically thin plasma, whose density must be above 0.1 g cm^{-3}. If the radiated power is increased, line radiation will again cause the curve labeled "Radiation > Convection" to be curved upward as density decreases, so that the "desired regime" might possibly be extended to lower densities and temperatures. However, the zone satisfying equation (37) would nevertheless be rather narrow, and very detailed modeling would be necessary to establish the feasibility of such a system. Line radiation might also be increased by doping the plasma. Based on Figure 4, it appears that one could produce a layer of plasma with a density of a few tenths of a gram per cubic centimeter, and a temperature of a few hundred electron volts that might collapse an order of magnitude or two in size through radiative cooling. Recent simulations with the two-dimensional radiative hydrodynamics code LASNEX corroborate this (Estabrook 1998).

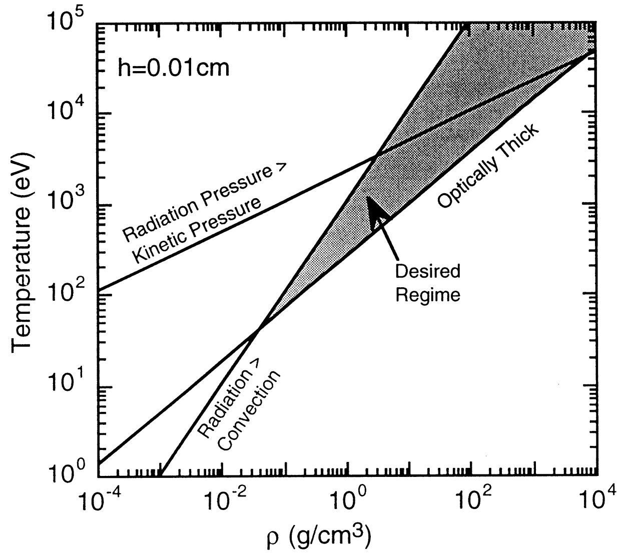

FIG. 4.—On the spatial scales of laboratory laser experiments, the system must be quite warm before the system becomes optically thin and radiation can dominate convection. Under these conditions, very high temperatures would be required for the radiation pressure to exceed the kinetic pressure. This figure is based on eqs. (37) and (38).

It is also of some interest to find conditions under which the radiation pressure $4\sigma T^4/3c$ (eqs. [32] and [33]) will exceed the gas-kinetic pressure $n_i\,T(Z+1)$, This condition is

$$[T(\mathrm{eV})]^3 > 2.1 \times 10^{10}\,\frac{Z+1}{A}\,\rho(\mathrm{g\ cm^{-3}})\,, \qquad (38)$$

and is also shown in Figure 4. The effect of the radiation pressure on the dynamics of the plasma will be most significant if this condition holds and the plasma is optically thick. From Figure 4 and equation (37), to achieve this for practical densities (≤ 10 g cm^{-3}) would require increasing h, and thus would involve a much larger experimental system that those of the 0.01 cm scale discussed here.

4. CONCLUSION

While all phases of SN explosions and SNR development are commonly modeled with hydrodynamic models, the justification for doing so changes. In the first phase ($t \sim$ 1000–40,000 s) the plasma is very strongly collisional, while later on magnetic fields are required to localize the particles so that the plasma behaves like a hydrodynamic fluid. We have evaluated the conditions under which a laboratory experiment can reasonably simulate SN and SNR phenomena. The laboratory and the astrophysical systems must be hydrodynamically similar, which involves having both a similar dimensionless shape and approximately equal values of the similarity parameter $v(\rho/p)^{1/2}$. In addition, both the laboratory and the astrophysical systems must satisfy a number of dissipation criteria, such as negligible heat conduction, viscosity, and radiation. We have also discussed the requirements on the equation of state. On a sufficiently small spatial scale, which we have identified, the similarity between the two systems will break down and their behavior will differ.

From this analysis, we conclude that there exists a very broad similarity that allows one to simulate SN and SNR phenomena in the laboratory, including the effects of three-dimensional initial perturbations and compressibility. Simulation experiments in this parameter domain can be directly mapped to the SN case by scale transformation.

This work was performed under the auspices of the US Department of Energy by Lawrence Livermore National Laboratory under contract W-7405-ENG-48 and with support from the University of Michigan.

REFERENCES

Arnett, D., Fryxell, B., & Muller, E. 1989, ApJ, 341, 63
Arnett, W. D., Bahcall, J. N., Kirschner, R. P., & Woosley, S. E. 1989, ARA&A, 27, 629
Blondin, J. M., Fryxell, B. A., & Königl, A. 1990, ApJ, 360, 370
Book, D. L. 1987, NRL Plasma Formulary (Washington, DC: Naval Research Laboratory)
Borkowski, K. J., Blondin, J. M., & McCray, R. 1997, ApJ, 477, 281
Braginski, S. I. 1965, in Reviews of Plasma Physics (New York: Consultants Bureau), 205
Chandrasekhar, S. 1961, Hydrodynamic and Hydromagnetic Stability (New York: Dover)
Chevalier, R. A. 1982, ApJ, 259, 302
———. 1992, Nature, 355, 691
———. 1997, Science, 276, 1374
Chevalier, R. A., Blondin, J. M., & Emmering, R. T. 1992, ApJ, 392, 118
Chevalier, R. A., & Fransson, C. 1994, ApJ, 420, 268
Chevalier, R. A., & Luo, D. 1994, ApJ, 421, 225
Drake, R. P., Carroll, J. J. III, Estabrook, K., Glendinning, S. G., Remington, B. A., Wallace, R., & McCray, R. 1998, ApJ, 500, L157
Duffy, P., Ball, L., & Kirk, J. G. 1995, ApJ, 447, 364
Ellison, D. C., & Reynolds, S. P. 1991, ApJ, 382, 242
Estabrook, K., et al. 1998, Bull. Am. Phys. Soc., 42, 2017
Fransson, C. 1984, A&A, 133, 264
Hillebrandt, W., & Höflich, P. 1989, Rep. Prog. Phys., 52, 1421
Hillebrandt, W., Höflich, P., Truran, J. W., & Weiss, A. 1987, Nature, 327, 597
Jeans, J. H. 1926a, MNRAS, 86, 328
———. 1926b, MNRAS, 86, 444
Jun, B. I., & Norman, M. L. 1996, ApJ, 465, 800
Kane, J., Arnett, D., Remington, B. A., Glendinning, S. G., Castor, J., Wallace, R., Rubenchik, A., & Fryxell, B. A. 1997, ApJ, 478, L75
Kilkenny, J. D., et al. 1994, Phys. Plasmas, 1, 1379
Kirk, J. G., & Wassman, M. 1992, A&A, 254, 167
Landau, L. D., & Lifshitz, E. M. 1987, Fluid Mechanics (Oxford: Pergamon)
Liang, E. 1996, in Proc. LLNL Conf. 960297 (Livermore: LLNL), 151
Luo, D., McCray, R., & Slavin, J. 1994, ApJ, 430, 264
Masai, K., & Nomoto, K. 1994, ApJ, 424, 924
McCray, R. 1993, ARA&A, 31, 175
Muller, E., Hillebrandt, W., Orio M., & Höflich, P. 1989, A&A, 220, 167
Muller, E., Fryxell, B., & Arnett, D. 1991, A&A, 251, 505
Remington, B. A., et al. 1997a, Phys. Plasmas, 4, 1994
———. 1997b, in Proc. Symp. on Supernova 1987a—Ten Years After, in press.
Schmidt, G. 1966, Physics of High Temperature Plasmas (New York and London: Academic)
Sedov, L. I. 1997, Mechanics of Continuous Media (Singapore: World Scientific)
Shigeyama, T., Nomoto, K., & Hashimoto, M. 1988, A&A, 196, 141
Sutherland, R. S., & Dopita, M. A. 1993, ApJS, 88, 253
Suzuki, T., Shigeyama, T., & Nomoto, K. 1993, A&A, 274, 883
Thomas, L. H. 1930, Quant. J. Math., 1, 239
Woosley, S. E., Pinto, P. A., & Ensman, L. 1988, ApJ, 324, 466
Zeldovich, Y. B., & Raiser, Y. P. 1966, Physics of Shock Waves and High-Temperature Hydrodynamic Phenomena (New York: Academic)

THE ASTROPHYSICAL JOURNAL, 698:2144, 2009 June 20 doi:10.1088/0004-637X/698/2/2144

ERRATUM: "SIMILARITY CRITERIA FOR THE LABORATORY SIMULATION OF SUPERNOVA HYDRODYNAMICS" (1999, ApJ, 518, 821)

D. D. RYUTOV, R. P. DRAKE[1], J. KANE, E. LIANG[2], B. A. REMINGTON, AND W. M. WOOD-VASEY[3]
Lawrence Livermore National Laboratory, Livermore, CA 94551, USA

We have discovered an error in one of the numerical examples presented in Table 2 of our paper (p. 828). Specifically, the localization parameter l_c/h for the laboratory experiment, presented in the right-most column of Table 2, should be equal to 2×10^{-6}, not to 1.1×10^{-8}. (Input parameters used for evaluating l_c/h via Equation (9) are taken from Table 1, $T = 3.8$ eV, $n_i = 5.5 \times 10^{22}$ cm^{-3}; the parameter $\Lambda = 1$ is taken from the bottom line of Table 2.) This error does not affect our further discussion and our conclusions.

Prepared by LLNL under Contract DE-AC52-07NA27344.

[1] University of Michigan, Ann Arbor, MI 48105.
[2] Rice University, Houston, TX 77005.
[3] University of Pittsburgh, Physics and Astronomy, Pittsburgh, PA 15260.